Operation and design issues of a doubly fed induction generator stator connected to a dc net by a diode rectifier

Matteo F. Iacchetti[1], *Gil D. Marques*[2], *Roberto Perini*[1]

[1]*Dipartimento di Energia, Politecnico di Milano, via Lambruschini 4, 20156 Milan, Italy*

[2]*INESC-ID, DEEC, Instituto Superior Técnico (IST), University of Lisbon, Avenue Rovisco Pais, no 1, 1049-001 Lisbon, Portugal*

E-mail: matteo.iacchetti@polimi.it

Received on 20th December 2013
Revised on 20th March 2014
Accepted on 27th March 2014

Nomenclature

A_{sn}, A_{rn}	stator, rotor rated power, W
$\bar{i}_s$, $\bar{i}_r$	stator, rotor current space vector, pu
R_s, R_r	stator, rotor resistance, pu
L_s, L_{kr}	stator, Γ-model rotor inductance, pu
Ps	stator power, pu
Te, T_L	electromagnetic, load torque, pu
$\bar{v}_s$, $\bar{v}_r$	stator, rotor voltage space vectors, pu
V_{dc}	dc-bus voltage, pu
γ	phase shift between $\bar{v}_s$ and $\bar{i}_r$, rad
θ_s, θ_r	d-axis position with respect to the stator, rotor, rad
$\bar{\psi}_s$, $\bar{\psi}_r$	stator, rotor flux linkage space vector, pu
ω_b	rated angular frequency, rad/s
ω_s, ω_r, ω_m	stator frequency, slip speed, rotor speed, pu

Superscripts

$\bar{x}$	complex quantity
*	set-point value

Subscripts

a, b, c	phases
d, q	oriented frame axes
s, r, R	stator, rotor, rotor in the Γ equivalent circuit
α, β	stationary axes
$\underline{x}$	conjugate of $\bar{x}$

1 Introduction

In variable-speed wind energy conversion system (WECS), the doubly fed induction generator (DFIG) has been widely used in order to reduce the cost of the power electronics [1]. Most of the studies in the literature consider the connection to an ac mains or the standalone configuration aimed to feed ac loads. The basic control issues of the rotor and grid side converters have been analysed in [2, 3]. Several studies have been also devoted to improve the low-voltage ride-through capability [4, 5] and the operation under asymmetrical or distorted load conditions [6–10]. Also, the sensorless control has been deeply investigated and techniques for the encoder-less control able to achieve a stable behaviour also at synchronism have been proposed [11–16].

Even if ac power systems are diffused everywhere, today there is also growing interest towards the integration of several sources and storages in a distributed generation system by using dc nets [17–20]. No reactive power circulation, simpler paralleling procedures, as well as the possibility to minimise the conversion stages are some advantages of such a layout.

An ac generator can be connected to a dc bus simply by a diode rectifier. However, in order to achieve an acceptable regulation, an additional full power dc–dc converter can be often required, as it happens for instance with permanent magnet synchronous generators [21, 22]. The field regulated synchronous generator (FRSG) connected by a diode

rectifier to the dc grid allows a considerable reduction of the cost of the controlled converters, because, besides the diode rectifier rated to the full power, it needs only a reduced-power dc–dc rotor converter. However, since the constant dc voltage implies a roughly constant electromotive force (EMF), the FRSG must work with a growing stator flux at low speed. As a consequence, the magnetic circuit of a FRSG must be considerably oversized with respect to the flux demand at the rated speed and power. As an alternative, the FRSG can be replaced by a DFIG which can be controlled by a unique reduced-power rotor-side inverter, whose dc bus is connected in parallel to the stator-side diode rectifier. Even if the DFIG implies a higher cost of the power electronics (inverter) with respect to the FRSG (chopper), it can regulate the stator frequency independently of the rotor speed, so that it can work with a stator flux near the rated value even at low speed, resulting in a less bulky generator. Since in a DFIG connected to a diode rectifier the frequency is neither imposed by an ac mains nor by the rotor speed, a proper regulation must be implemented. A layout based on a single PWM converter has been studied in [23], where the DFIG feeds a standalone ac load and the rotor inverter is only connected to a battery. The layout consisting of a single inverter and a diode rectifier has been proposed in [24], where a vector control scheme in the stator flux linkage frame has been considered: the frequency is regulated by acting on the *d*-axis rotor current by an additional proportional-integral (PI) controller and a frequency detector. Owing to the presence of only a single and reduced-power PWM converter, the aforementioned system reduces the cost and the bulk of the power electronics with respect to the traditional configuration based on the back-to-back converter. Under the point of view of the control, if the dc voltage is imposed by a dc grid, the system cannot be treated simply as an ac standalone system feeding a non-linear load [10, 13]. In fact, in the system considered in this paper, the DFIG can be controlled in such a way to extract the maximum power from the wind stream, exactly as in an ac-grid connected DFIG. The main difference with respect to DFIGs connected to an ac grid is the need of the frequency control. Apart from the integration of the DFIG to other sources or storages through a unique dc bus, this scheme could be directly applied in small wind farms, by using a common dc link with a voltage of few kV. The dc output can also directly supply an inverter feeding a high-frequency transformer and a diode rectifier, in order to connect the system to a high voltage dc grid [25].

The discussion in [24] mainly focuses on the control issues, whereas the aspects related to the derating of the DFIG because of the harmonics as well as the design requirements for the DFIG in this special application have not been discussed at all. These matters are analysed in this paper by considering a simple control technique, where the rotor current space vector is forced to move along a circular trajectory at constant speed in order to achieve a constant stator frequency. The amplitude of the rotor current is regulated to vary the power delivered to the dc bus. The paper proposes an analytical model for the steady-state operation and deduces the most proper design specifications for the DFIG in the considered application. The work is organised as follows. Section 2 presents the system layout and the DFIG equations. Section 3 introduces the control scheme and provides both a steady-state analysis and the details of the implementation. The design issues concerning the choice of the DFIG rated voltage, of the turns ratio, as well as of the stator and rotor apparent powers are analysed in Section 4 by considering the distorted waveforms. Sections 5 and 6 show the simulation and the experimental results obtained by a small power prototype.

2 System layout and DFIG equations

The system considered in this paper is reported in Fig. 1*a*. A diode rectifier is connected to the stator and to a dc net, which simultaneously feeds the rotor-side inverter. No additional PWM converters are needed, differently from DFIGs connected to an ac grid, where a back-to-back converter consisting of two PWM converters is used.

The Γ equivalent circuit in Fig. 1*b* is considered in this paper. With respect to a generic frame *dq*, the DFIG equations in pu are

$$\bar{v}_{\mathrm{s}} = -R_{\mathrm{s}}\bar{i}_{\mathrm{s}} + \frac{1}{\omega_b}\frac{\mathrm{d}\bar{\psi}_{\mathrm{s}}}{\mathrm{d}t} + \mathrm{j}\frac{1}{\omega_b}\frac{\mathrm{d}\theta_{\mathrm{s}}}{\mathrm{d}t}\bar{\psi}_{\mathrm{s}} \tag{1}$$

$$\bar{v}_{\mathrm{R}} = R_{\mathrm{R}}\bar{i}_{\mathrm{R}} + \frac{1}{\omega_b}\frac{\mathrm{d}\bar{\psi}_{\mathrm{R}}}{\mathrm{d}t} + \mathrm{j}\frac{1}{\omega_b}\frac{\mathrm{d}\theta_{\mathrm{r}}}{\mathrm{d}t}\bar{\psi}_{\mathrm{R}} \tag{2}$$

$$t_{\mathrm{e}} = \mathrm{Im}\left(\bar{\psi}_{\mathrm{s}}\underline{i_{\boldsymbol{R}}}\right), \quad \bar{i}_{\mu} = \left(\bar{i}_{\mathrm{R}} - \bar{i}_{\mathrm{s}}\right) \tag{3}$$

$$\bar{\psi}_{\mathrm{s}} = L_{\mathrm{s}}\bar{i}_{\mu}, \quad \bar{\psi}_{\mathrm{R}} = \bar{\psi}_{\mathrm{s}} + L_{k\mathrm{r}}\bar{i}_{\mathrm{R}} \tag{4}$$

where rotor quantities in the Γ model are defined as

$$\bar{\psi}_{\mathrm{R}} = \frac{L_{\mathrm{s}}}{M}\bar{\psi}_{\mathrm{r}}, \quad \bar{v}_{\mathrm{R}} = \frac{L_{\mathrm{s}}}{M}\bar{v}_{\mathrm{r}}, \quad \bar{i}_{\mathrm{R}} = \frac{M}{L_{\mathrm{s}}}\bar{i}_{\mathrm{r}} \tag{5}$$

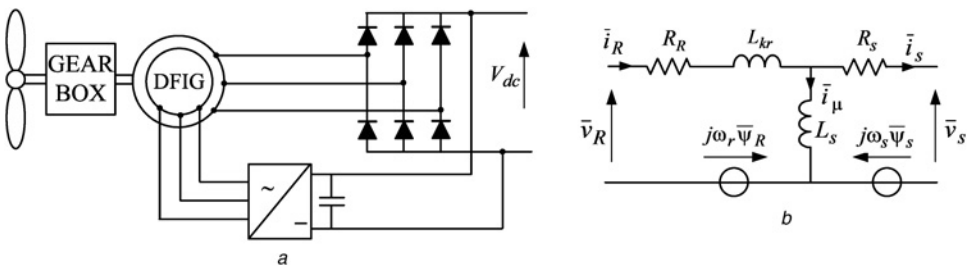

Fig. 1 *DFIG connected to a dc grid by a diode rectifier*

a Layout of the system
b Γ equivalent circuit

3 Control scheme and analysis

3.1 General principle

In this paper, the dc voltage V_{dc} is assumed to be controlled by other devices connected to the dc net. Thus, the aim of the control system is the regulation of the frequency and of the power delivered to the dc net. The frequency is to be regulated near the rated value of the DFIG, especially at low speed, in order to limit the flux amplitude and the weight of the machine.

The proposed control method for the system in Fig. 1*a* consists in forcing along a circular trajectory at constant speed the rotor current space vector $\bar{i}_r$ in such a way to obtain the rated stator frequency. Simultaneously, the magnitude of $\bar{i}_r$ is adjusted in order to regulate the stator power. Fig. 2*a* shows the reference frames and the space vectors involved in the control. The reference angle θ_s^* is generated by integrating the rated angular frequency and fixes the position of the control dq frame. A preliminary steady-state analysis of the system in Fig. 1*a* with a sinusoidal current flowing in the rotor is preparatory in order to discuss the details of the control implementation and the most proper design specifications of the DFIG. Fig. 2*b* shows the equivalent circuit in the stator frame: the rotor is represented by a current generator, and the stator resistance is neglected.

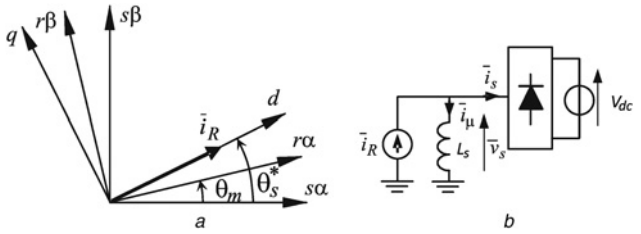

Fig. 2 *Control scheme and analysis*

a Reference frames for the control of the DFIG
b Reduced equivalent circuit in the stator frame

3.2 Steady-state analysis

If the magnitude of the rotor current space vector is large enough, the rectifier operates in continuous conduction mode (CCM, or mode 3/3), and the stator terminal voltages are three-step square waves displaced by $2\pi/3$ rad [26, 27]. Thus, the equivalent circuit in Fig. 2*b* can be redrawn as in Fig. 3*a*. The waveforms related to the phase '*a*' in the operation in CCM are shown in Fig. 3*b*, where the zero phase is assumed for the sinusoidal rotor current.

Fig. 3*b* shows that the zero crossings of the rotor current lags the zero crossings of the stator voltage by the angle γ. In CCM, the phase stator flux waveform is immediately obtained by integrating the three-step square wave and is a linear piecewise line. In particular, the amplitude of the first harmonic component of the stator terminal voltage and the peak value of the stator flux linkage in pu are given by

$$\hat{V}_{s1} = \frac{2}{\pi} V_{dc} \quad \hat{\psi}_s = \frac{2\pi}{9} \frac{V_{dc}}{\omega_s} \tag{6}$$

Equation (6) provides a good approximation also in the operation in mode 2/3 [26].

Owing to (4), the magnetising current $i_{\mu a}$ has the same waveform of the stator flux linkage ψ_{sa}, and, in CCM, the stator current crosses the zero together with the stator terminal voltage. This means that, for $\zeta = \pi - \gamma$, the rotor

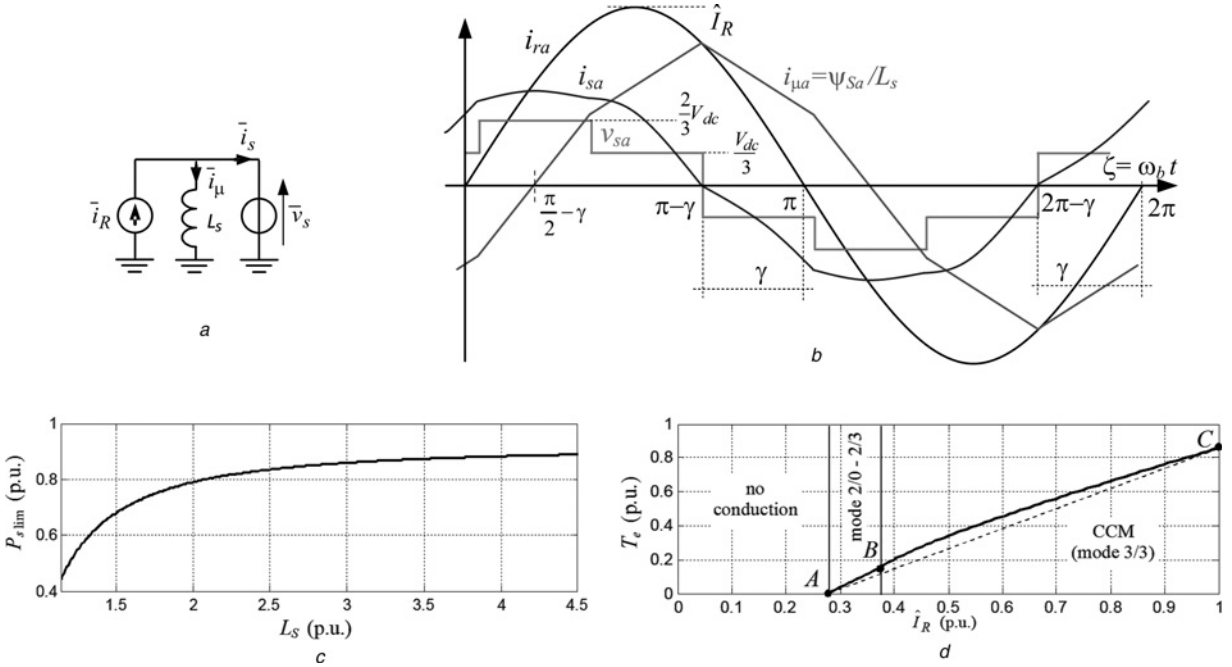

Fig. 3 *Operation of the system in CCM*

a Reduced equivalent circuit
b Waveforms of the rotor current, stator terminal voltage, magnetising and stator current in the phase *a*
c Maximum active power in rated condition as a function of the stator inductance (10)
d Relation between the average electromagnetic torque and the amplitude of the rotor current (14)

current equals the magnetisation current. Thus

$$\hat{I}_R \sin(\pi - \gamma) = \frac{2\pi}{9}\frac{V_{dc}}{\omega_s L_s} \Rightarrow \sin\gamma = \frac{2\pi}{9}\frac{V_{dc}}{\omega_s L_s \hat{I}_R} \quad (7)$$

For the operation in CCM, the slope of the straight line of $i_{\mu a}$ at $\zeta = \pi - \gamma$ cannot be higher (in absolute value) than the local slope of i_{Ra}. Hence, the existence condition of mode 3/3 is

$$\frac{1}{\omega_s L_s}\frac{V_{dc}}{3} \le \hat{I}_R|\cos\gamma| = \hat{I}_R\sqrt{1-\sin^2\gamma} \quad (8)$$

By replacing (7) in the square root of (8), after some manipulations the existence condition for the mode 3/3 is obtained

$$\frac{\omega_s L_s \hat{I}_R}{V_{dc}} \ge \frac{\sqrt{9+4\pi^2}}{9} \quad (9)$$

Since the stator resistance as well as the losses in the diode rectifier have been neglected, the pu dc power equals the pu stator power P_s. Using also (7b) yields

$$P_s = \hat{V}_{s1}\hat{I}_R\cos\gamma = \frac{2}{\pi}V_{dc}\hat{I}_R\sqrt{1-\left(\frac{2\pi}{9}\frac{V_{dc}}{\omega_s L_s \hat{I}_R}\right)^2} \quad (10)$$

To evaluate the maximum power which can be delivered to the dc bus, the capability limits of the DFIG should be considered. Hereafter, the constraints related to the saturation and to the current limits will be taken into account. As far as the limitation of the saturation level is concerned, the peak value of the stator flux linkage (6) should not overcome the limit value 1 pu. This condition provides the maximum tolerable pu value of the dc-bus voltage

$$V_{dc\,lim} = \frac{9}{2\pi}\omega_s \cong 1.432\,\text{pu} \quad (11)$$

where the rated frequency ($\omega_s = 1$ pu) has been assumed. By using the value in (11), the magnetic circuit of the DFIG works near the optimal condition.

As far as the current limits are concerned, the most restrictive constraint regards the rotor current, because, in the layout of Fig. 1*a*, the rotor necessarily provides also the whole magnetisation current. Thus, the DFIG should be designed for a rated rotor magnetomotive force (MMF) higher than the stator one. However, the global size of medium–large DFIGs is rather independent of the side from which the magnetising power is supplied. In fact, the reduction of the available space for the rotor slots because of the curvature is not quite significant, provided that the air gap diameter is not too small. It should be noted that, in DFIGs with a high pole number, limiting the pu magnetisation current (which is inversely proportional to the pole pitch [30]) already assures a considerable air gap diameter. Moreover, since in a design for the proposed application the amount of the stator copper is lower than the one of the rotor, the stator slot height can be reduced and the air gap diameter can be slightly increased, being the external diameter also slightly increased. As an alternative, the rectifier can be connected to the rotor windings and the inverter to the stator ones, where the allowable space for the slots is slightly higher.

If the inverter is connected to the rotor, the higher rated rotor MMF in a proper DFIG design for the considered application suggests to use as base current for the pu notation the rotor rated current referred to the stator (i.e. $I_b = I_{rn}/n_{12}$). The current capability region of the rotor is defined by $\hat{I}_R \le 1$ pu.

By replacing (11) in (9), the existence condition of the CCM becomes

$$\hat{I}_R \ge \frac{\sqrt{9+4\pi^2}}{2\pi}\frac{1}{L_s} \cong \frac{1.108}{L_s} \quad (12)$$

By considering that ordinarily $1.5 \le L_s \le 4.5$ pu (from small to large DFIGs), it can be concluded from (12) that the rectifier always operates in CCM even for a moderate (or low, in large DFIGs) level of the rotor current, if the control is able to impose a sinusoidal rotor current. For instance, if $L_s = 3$ pu, the boundary current above which the system operates in CCM is $\hat{I}_R = 0.37$ pu.

Replacing (11) in (10) with $\hat{I}_R = 1$ pu yields the maximum pu stator power which can be delivered to the dc bus at the boundary of the rotor current and flux capability of the DFIG and at the rated frequency ($\omega_s = 1$ pu)

$$P_{s\,lim} = \frac{9}{\pi^2}\sqrt{1-\left(\frac{1}{L_s}\right)^2} \quad (13)$$

The curve $P_{s\,lim}(L_s)$ (13) is plotted in Fig. 3*c*: for $1.5 \le L_s \le 4.5$ pu, the limit power belongs to the range $0.68 \le P_{s\,lim} \le 0.89$ pu. Fig. 3*c* gives an estimation of the derating of the DFIG because of the stator current harmonics and takes into account also the contribution of the magnetisation current to the rotor current. With respect to the sinusoidal operation, where the maximum power which could be delivered by the stator when $\hat{I}_R = 1$ pu is $P_{s\,lim} = \left(1 - 1/L_s^2\right)^{1/2}$, (13) shows that a penalty factor equal to $9/\pi^2 \simeq 0.91$ must be considered if the DFIG feeds a diode bridge. This means that a DFIG designed for the sinusoidal operation should be derated when it has to feed a diode rectifier as in the scheme in Fig. 1*a*. Alternatively, for a given required stator power, the DFIG should be specifically designed by considering a higher rated apparent power with respect to the sinusoidal operation: this concept is developed in Section 4.

As last issue, it is interesting to relate the average electromagnetic torque to the amplitude $\hat{I}_R$ of the rotor current and to the level of the dc voltage. To this purpose, the steady-state relation $P_s = \omega_s T_e$ can be replaced in (10), which has to be solved with respect to T_e, so that

$$T_e = \frac{2}{\pi}\frac{V_{dc}}{\omega_s}\hat{I}_R\sqrt{1-\left(\frac{2\pi V_{dc}}{9\omega_s L_s \hat{I}_R}\right)^2}, \text{ if } \hat{I}_R \ge \frac{\sqrt{9+4\pi^2}}{2\pi L_s} \quad (14)$$

If $\sqrt{3}\omega_s L_s \hat{I}_R < V_{dc}$, that is, $\hat{I}_R < V_{dc}/\sqrt{3}\omega_s L_s$, the diode rectifier is blocked and the average torque is zero. In the range $V_{dc}/\sqrt{3}(\omega_s L_s) < \hat{I}_R < (9+4p^2)^{1/2}/(2\pi L_s)$ where modes other than 3/3 exist, a linear interpolation can be used to approximate the expression of the torque $T_e(\hat{I}_R)$. Fig. 3*d* shows the resulting graphic when $L_s = 3$ pu, $\omega_s = 1$ pu and when V_{dc} is given by (11): CCM exists for $\hat{I}_R > 0.37$ pu.

3.3 Implementation of the control

The control scheme considered in this paper is reported in Fig. 4 and is based on two axis control loops for the rotor current.

The integration of the reference (rated) frequency ω_s^* produces the reference angle θ_s^*, which defines the position of the control dq frame. The d-axis is aligned along the rotor current space vector by setting to zero the reference q-axis rotor current, that is, $i_{rq}^* = 0$. The reference magnitude $\hat{I}_R^*$ of the rotor current space vector could be obtained from the reference average torque by inverting the relation T_e ($\hat{I}_R$) (14) and by using a linear interpolation outside the CCM region. However, as shown in Fig. 3*d*, the trend of T_e ($\hat{I}_R$) in the whole operating region is well approximated by a straight line which connects the two extreme points A and C. As previously mentioned, the conduction of the diode bridge starts when $\hat{I}_R = V_{dc}/\sqrt{3}\omega_s L_s = \hat{I}_{RA}^*$, whereas the torque T_{eC} delivered when $\hat{I}_R = \hat{I}_{RC}^* = 1$ pu is obtained by replacing $\hat{I}_R = 1$ pu in (14). Thus, the approximated straight line which connects the points A and C in Fig. 3*b* is represented by

$$\hat{I}_R^*(T_e^*) \cong \hat{I}_{RA}^* + \frac{\hat{I}_{RC}^* - \hat{I}_{RA}^*}{T_{eC}} T_e^* = \frac{V_{dc}}{\sqrt{3}\omega_s L_s} + \frac{\pi\left(3\omega_s L_s - \sqrt{3}V_{dc}\right)}{6L_s V_{dc}\sqrt{1 - \left(\frac{2\pi}{9}\frac{V_{dc}}{\omega_s L_s}\right)^2}} T_e^* \quad (15)$$

The slope coefficient in (15) is a non-linear function of V_{dc} which can be linearised around the optimal value of V_{dc} in (11).

The reference average torque T_e^* is provided by the speed controller PI$_\omega$: in practice, the reference speed could be set in order to maximise the turbine power [28]. The torque in (15) is related to the operation as generator and is positive. Hence, a negative sign is required in the speed loop in Fig. 8, because the speed regulator provides a motoring reference torque.

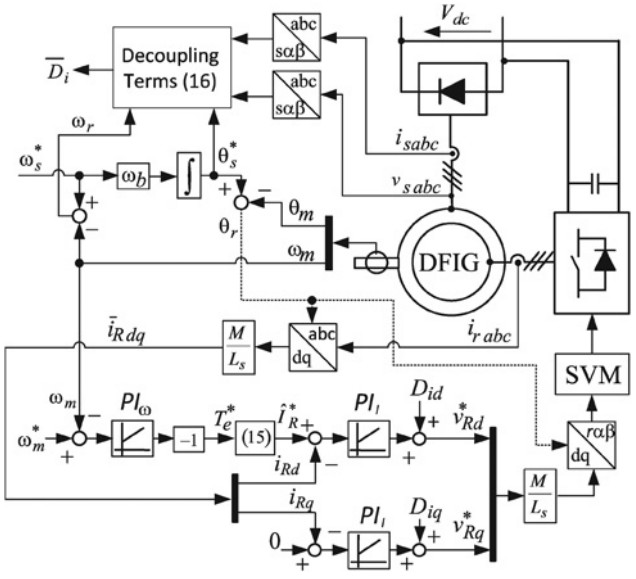

Fig. 4 *Proposed control scheme*

The decoupling and feed-forward term $\bar{D}_i$ for the current loops is deduced by using (1)–(4)

$$\bar{D}_i = \bar{v}_s + j\omega_r L_{kr}\bar{i}_R - j\omega_m\bar{\psi}_s - \frac{R_s}{L_s}\bar{\psi}_s \quad (16)$$

The stator flux linkage $\bar{\psi}_s$ is evaluated by an approximated integration of the stator EMFs using a low-pass filter [11].

4 Design specifications for the DFIG

Hereafter, it is assumed that the DFIG has to be designed to operate connected to a dc grid with a given voltage $V_{dc}^{(Volt)}$ (in volt) and it is required to convert a given turbine power P_T (in Watt) at the rated turbine speed of 1.33 pu (i.e. with a slip equal to −0.33). Hence, the most proper rated stator voltage and stator/rotor turns ratio, as well as the stator and rotor apparent powers of the machine should be defined.

Starting from (11), which provides the optimal pu dc voltage, the stator rated voltage V_{sn} (line-to-line) is obtained

$$V_{dc} = \frac{V_{dc}^{(Volt)}}{\sqrt{2}V_{sn}/\sqrt{3}} = \frac{9}{2\pi} \Rightarrow V_{sn} = \sqrt{\frac{2}{3}}\frac{\pi}{3}V_{dc}^{(Volt)} \quad (17)$$

Table 1 collects the resulting optimal value of V_{sn} for some values of V_{dc}.

It should be noted that (17) is slightly higher than the peak value of the stator voltage [i.e. $(2/3)V_{dc}^{(Volt)}$]: thus, using (17) implicitly guarantees the insulation adequacy.

The turns ratio n_{12} should be chosen by considering that the rotor voltage is distorted, mainly because of the distorted stator voltage and stator flux linkage. The maximum amplitude of the rotor voltage space vector is evaluated with the simplified equivalent circuit in Fig. 5, where the resistances have been neglected.

By considering the waveforms in Fig. 3*b*, and $\omega_m = 1.33$ pu (i.e. $s = -0.33$), the following relations hold for $\zeta = (2\pi - \gamma)^+$

$$v_{s s\alpha} = \frac{V_{dc}}{3}, \quad v_{s s\beta} = -\frac{V_{dc}}{\sqrt{3}}, \quad \psi_{s s\alpha} = -\frac{2\pi}{9}\frac{V_{dc}}{\omega_s}, \quad \psi_{s s\beta} = 0 \quad (18)$$

In Fig. 5, the voltage drop across the leakage inductance L_{kr} gives a negligible contribution to $|\bar{v}_R|$, because it is almost in quadrature with respect to $\bar{v}_x$, and its modulus is small. Thus, the maximum amplitude of the rotor voltage space

Table 1 Optimal value of V_{sn} according to (17)

V_{dc}, V	400	600	1500	3000	6000
V_{sn}, V	342	513	1282	2565	5130

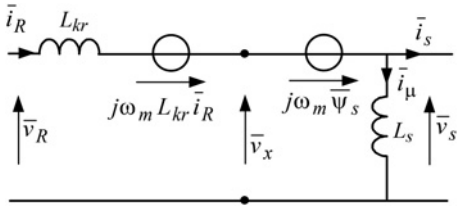

Fig. 5 *Simplified equivalent circuit set in the stator frame, used to calculate the maximum amplitude of the rotor voltage space vector*

vector can be approximated as $|\bar{v}_R|_{max} \simeq |\bar{v}_x|_{max}$. Since, because of Fig. 5, the maximum modulus of the space vector $\bar{v}_x = \bar{v}_s - j\omega_m \bar{\psi}_s$ is

$$|\bar{v}_x|_{max} = \sqrt{\left(v_{s\,s\alpha} + \omega_m \psi_{s\,s\beta}\right)^2 + \left(v_{s\,s\beta} - \omega_m \psi_{s\,s\alpha}\right)^2} \quad (19)$$

from (18) and (19) it follows

$$|\bar{v}_R|_{max} \cong |\bar{v}_x|_{max} = \sqrt{\frac{1}{9} + \left(-\frac{1}{\sqrt{3}} + \frac{2\pi}{9}\omega_m\right)^2} V_{dc} \cong 0.48\ V_{dc} \quad (20)$$

where $\omega_m = 1.33$ pu and $\omega_s = 1$ pu have been assumed.

By referring (20) to the rotor side using (5) and the turns ratio n_{12}, and by considering that the maximum amplitude of the voltage space vector achievable by the space vector modulation is $V_{dc}/\sqrt{3}$, the following inequality must be satisfied

$$\frac{M}{L_s}\frac{|\bar{v}_R|_{max}}{n_{12}} < \frac{V_{dc}}{\sqrt{3}} \Rightarrow n_{12} > 0.48\sqrt{3} = 0.83 \quad (21)$$

where the ratio M/L_s (<1) has been neglected.

Even if the inverter must operate only with a slip limited to ±0.33, the design of the DFIG should take into account the possibility to operate also with a unitary slip (for instance with open rotor windings and locked rotor, for testing purposes). Thus, it is reasonable to consider a design rotor apparent power A_{rn} equal to $\sqrt{3}V_{sn}\,(I_{rn}/n_{12}) = (1.5V_bI_b) = A_b$. Since, in the rated conditions of the turbine, the stator power is $P_T/1.33$, equating (13) to $(P_T/1.33)/A_b = (P_T/1.33)/A_{rn}$ gives the required rotor apparent power A_{sn}

$$A_{rn} = \frac{P_T/1.33}{P_{s\,lim}} = \frac{\pi^2}{9}\sqrt{\frac{L_s^2}{L_s^2 - 1}}\frac{P_T}{1.33} \quad (22)$$

where $L_s = 2.5$–4 pu, depending on the number of poles and on the size of the DFIG.

To find the stator apparent power A_{sn}, we need to estimate the pu root-mean-square value of the distorted stator current. This can be done by considering the waveforms in Fig. 3*b* and the relation $i_{sa} = i_{Ra} - i_{\mu a}$ from which it follows

$$I_{s\,rms}^2 = \frac{\hat{I}_R^2}{2} + I_{\mu\,rms}^2 - \frac{1}{\pi}\int_0^{2\pi} i_{\mu a}(\theta)\hat{I}_R \sin\theta \mathrm{d}\theta \quad (23)$$

The quantity $I_{\mu\,rms}^2$ can be directly calculated by considering the symmetry of the waveform $i_{\mu a}$ in Fig. 3*b*

$$I_{\mu\,rms}^2 = \frac{4}{2\pi}\int_{\frac{\pi}{2}-\gamma}^{\pi-\gamma} i_{\mu a}^2(\theta)\mathrm{d}\theta = \frac{5\pi^2}{243}\left(\frac{V_{dc}}{\omega_s L_s}\right)^2 \quad (24)$$

The integral in (23) can be rewritten using the new dummy variable $\theta' = \theta - (\pi/2 - \gamma)$, so that the relation $\sin\theta = \sin\gamma\ \sin\theta' - \cos\gamma\ \cos\theta'$ holds. With respect to the new variable

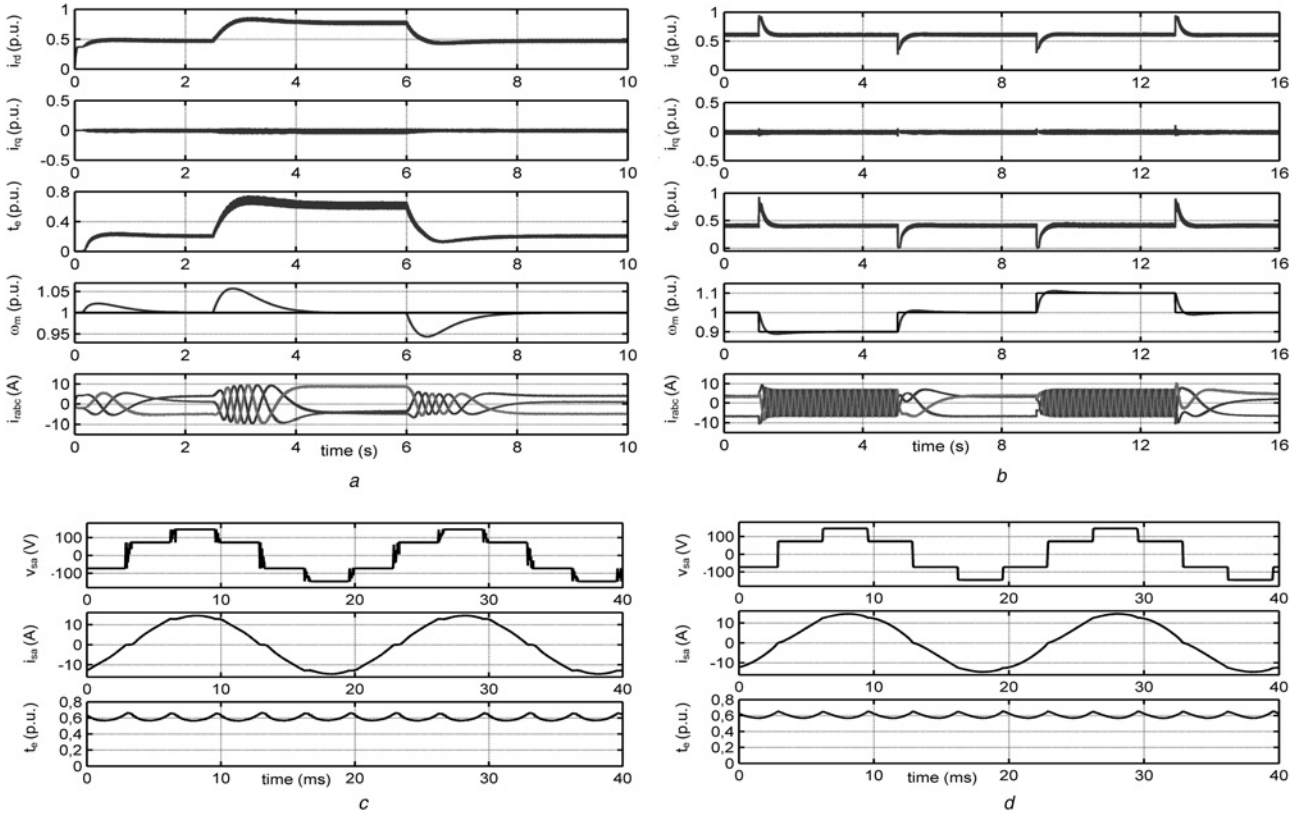

Fig. 6 *Simulation results*

a Response to a step in the moving torque
b Response to a step in the reference speed
c Steady stator voltage and current in the phase *a* and electromagnetic torque for $T_e = 0.6$ pu and with sample delay (100 ms)
d Steady-state waveforms without sample delay

θ', $i_{\mu a}$ contains only sine harmonics: hence, the third contribution in the second member of (23) corresponds to the first Fourier coefficient of $i_{\mu a}$ weighted by $\hat{I}_R \sin\gamma$, namely, by using (7)

$$\frac{1}{\pi}\int_0^{2\pi} i_{\mu a}\hat{I}_R \sin\theta \mathrm{d}\theta = \frac{4}{9}\left(\frac{V_{dc}}{\omega_s L_s}\right)^2 \tag{25}$$

By using (23)–(25), the following result is obtained

$$I_{s\,rms} = \sqrt{\frac{\hat{I}_R^2}{2} + \left(\frac{5\pi^2}{243} - \frac{4}{9}\right)\left(\frac{V_{dc}}{\omega_s L_s}\right)^2} \tag{26}$$

Thus, an estimation of A_{sn} is obtained from the ratio

$$\frac{A_{sn}}{A_{rn}} = \frac{I_{s\,rms}}{\hat{I}_R/\sqrt{2}} \cong \sqrt{1 - \frac{0.99}{L_s^2}} \tag{27}$$

where the last approximated equality has been obtained by considering the operation at the rated rotor current (i.e. $\hat{I}_R = 1$ pu) and with V_{dc} given by (11).

5 Simulation results

The performances of the control scheme in Fig. 4 have been evaluated by simulations on a 3.7 kW DFIG. A Simulink model has been used: the parameters are reported in the Appendix. In the considered machine, the rated apparent power of the rotor is 4.0 kVA, whereas the stator is rated to 5.27 kVA. According to (27), the rated rotor power required to fully exploit the rated power of the stator when it is connected to a diode rectifier would be 5.79 kVA, which is significantly higher than the rotor rated power of the used machine. Owing to this reason, in both the simulation and the experimental tests, the stator and the rotor have been exchanged (see also Fig. 7), so that the structure with the higher rated MMF is connected to the inverter, which supplies the whole magnetising current. This way, an appropriate margin for the torque component is available to perform meaningful tests with an adequate power level. Moreover, the turns ratio in the inverted configuration is 1/2.05 = 0.49, which is closer to the optimal value (21). Nevertheless, in order to simplify the comparison with the theory in Sections 3 and 4, also the notations of the rotor and stator have been inverted: now the subscripts 's' and 'r' depict a fictitious stator (bridge side, i.e. actual rotor) and rotor (inverter side, i.e. actual stator), respectively. An ideal inverter with a switching frequency of 10 kHz has been used, the speed and current loops have been designed with a bandwidth of 1 and 300 Hz, respectively. First-order delay blocks (time constant: 100 μs) have been inserted between the reference voltages and the inverter, in order to represent the sample and hold process. In accordance with (11) and by considering that the base voltage is $V_b = \sqrt{2}\cdot V_{rn}/\sqrt{3} = \sqrt{(2/3)}\cdot 185$ V, the dc-bus voltage has been set at 216 V according to (17). The base current is $I_b = \sqrt{2}(I_{rn}/n_{12}) =$ 23.2 A, and the maximum pu tolerable rms value of the stator current is $I_{sn}/I_b = I_{sn}/(\sqrt{2}I_{rn}/n_{12}) \simeq 0.76/\sqrt{2}$. Equating (26) to $0.76/\sqrt{2}$, using (11), and solving with respect to $\hat{I}_R$ gives $\hat{I}_R \simeq 0.87$ pu, which is the limit pu amplitude of the 'fictitious' rotor current (inverter side) compatible with the capability limits of the machine. Hence, the maximum average torque, predicted by (14) with $L_s = 2.27$ pu, $\hat{I}_R = 0.87$ pu and V_{dc} in (11), is $T_e \simeq 0.68$ pu.

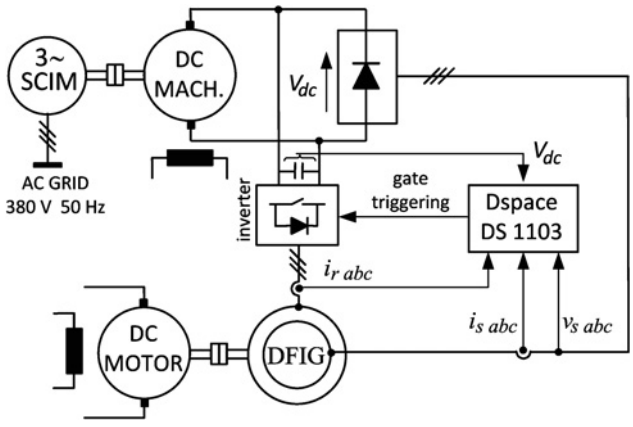

Fig. 7 *Simulated and experimental setup*

The simulation results are shown in Fig. 6. The starting of the control system and the behaviour during step changes in the moving torque are reported in Fig. 6*a*. The DFIG is initially driven at synchronism by the prime mover, and the control is enabled at $t = 0.05$ s. At $t = 0.15$ s, a step change in the moving torque to 0.2 pu is delivered, and at $t = 2.5$ s it is further increased to 0.6 pu. Finally, at $t = 6$ s, the torque is decreased to 0.2 pu. As a consequence of each step, the control adjusts the magnitude of the rotor current in order to produce the required torque: after each transient, the system is able to restore the rotor speed at 1 pu (set-point value).

Since the average i_{rq} is zero, the orientation is achieved in average: a sixth harmonic in the *dq* rotor currents occurs, as a consequence of the limited ability of the current controllers to track the high-order harmonics.

The response during step changes in the reference speed with a moving torque equal to 0.4 pu is shown in Fig. 6*b*: the speed controller restores the speed to the set-point value. Again, the system correctly tracks the reference stator frequency. In the initial instants of the acceleration transient, the reference torque reaches the zero value and is clamped to it: this can slow the response. In fact, because of the diode rectifier connected to the stator, the DFIG cannot produce an accelerating electromagnetic torque.

Fig. 6*c* shows the steady-state stator voltage and current (bridge side) as well as the instantaneous electromagnetic when its average value is $T_e = 0.6$ pu. The rotor frequency is 50 Hz, that is, it matches with the set-point value. The peak-to-peak torque ripple is about 0.1 pu for $T_e = 0.6$ pu. The rectifier is working very close to the CCM, even if (12) would predict full CCM already for $\hat{I}_R > 0.49$ pu. This discrepancy is mainly because of the sample delay, which worsens the compensation of the sixth harmonic component in the rotor current. To validate the theory, Fig. 6*d* shows the simulation results in the same conditions of Fig. 6*c*, but without the equivalent delay: now, CCM operation is achieved.

Finally, the theoretical relation (14) represented by the curve BC in Fig. 3*d*, has been validated by simulations, as shown in Table 2. The calculated values are very close to the simulated ones.

6 Experimental results

The experimental setup is illustrated in Fig. 7. The data of the 3.7 kW DFIG are reported in the Appendix: the rotor is driven by dc motor. As previously mentioned, the stator and the rotor

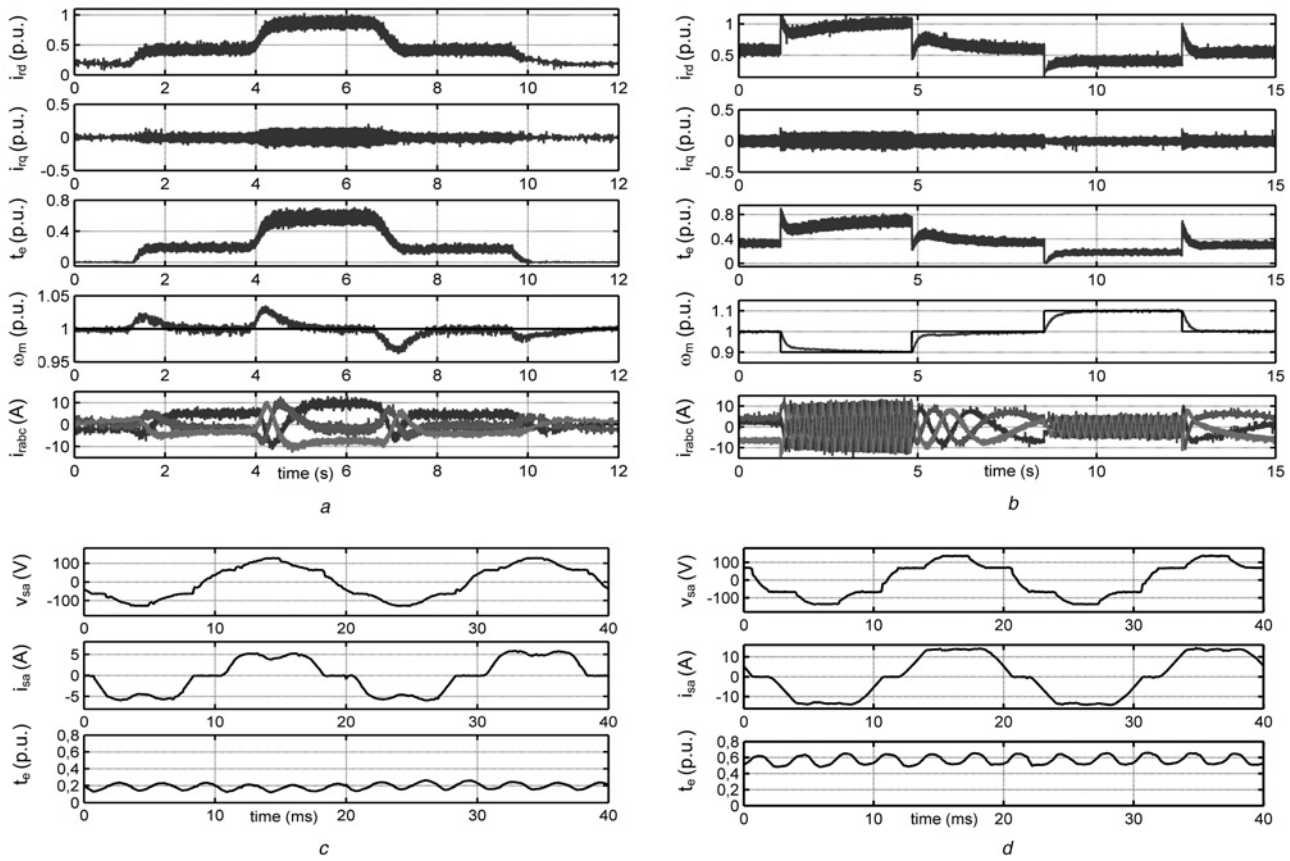

Fig. 8 *Simulation results*

a Behaviour after step changes in the moving torque from almost 0 to 0.2 pu, from 0.2 to 0.6 pu and vice versa
b Behaviour after step changes in the reference speed from 1 to 0.9 pu, from 1 to 1.1 pu and vice versa
c Steady stator voltage and current in the phase *a* and electromagnetic torque for $T_e = 0.2$ pu
d Steady stator voltage and current in the phase *a* and electromagnetic torque for $T_e = 0.6$ pu

connections have been exchanged, so that the control and the inverter act on the stator currents.

The dc net, which is shared by the inverter and the diode rectifier, has been obtained by a 30 kW dc machine coupled to a squirrel cage induction machine (SCIM) which is fed by the ac mains. The dc voltage has been set at 216 V.

A DSpace platform (DS 1103) has been used to implement the control routine (switching and sampling frequency: 10 kHz).

The instantaneous electromagnetic torque has been obtained from (3) set in the stator frame. The stator flux linkage has been evaluated by using the stator EMFs: an approximate integrator based on a low-pass filter has been implemented [11].

Fig. 8*a* shows the response of the control system during step variations of the moving torque applied by the dc motor. The torque is changed from almost 0 to 0.2 pu, and then from 0.2 to 0.6 pu and vice versa; the reference speed is set at 1 pu. The maximum delivered torque is about 0.6 pu (i.e. close to the limit torque compatible with the rated stator current). The control is able to track the reference speed and the frequency, as it can be deduced by observing the zero frequency of the rotor (inverter) currents at steady state. The system can also stably operate in the quiescent condition with no electromagnetic torque. The *dq* rotor (inverter) currents are affected by a significant ripple at 300 Hz. In spite of the designed bandwidth (300 Hz) of the current loops, the PI regulators are not able to fully compensate for the current ripple. The delay because of the sample and hold process causes a further worsen of the control, as pointed out in Section 5. This is confirmed also in Figs. 8*c* and *d*, which report the steady-state stator (rectifier) phase voltage and current as well as the electromagnetic torque, for two different levels of the average torque: namely 0.2 and 0.6 pu, respectively. The steady-state frequency corresponds to the set point (50 Hz), however, even with a high torque, the rectifier is still operating in mode 2/3, instead of CCM. The torque ripple increases with the load and equals 0.16 pu when the average torque is about 0.6 pu. A slight beat at 50 Hz affects the torque and is due to the low damping of the stator flux dynamics [29].

The behaviour of the system during step changes in the reference speed from 1.0 to 0.9 pu and from 1.0 to 1.1 pu is shown in Fig. 8*b*. In all the cases, the speed control correctly tracks the reference speed, in accordance to the bandwidth of the speed loop. The increase of the steady-state torque when the speed decreases is due to the mechanical characteristic of the separate excitation dc

Table 2 Comparison between (14) and the simulation results ($\omega_s = 1$ pu, $L_s = 3$ pu and $V_{dc} = 9/2\pi$, and $R_s = 0.01$ pu in the simulations)

T_e, pu	0.144	0.2	0.4	0.6	0.8
$\hat{I}_R$, pu [inverting (14)]	0.369	0.399	0.551	0.737	0.938
I_R, pu (simulations)	0.352	0.391	0.562	0.730	0.932

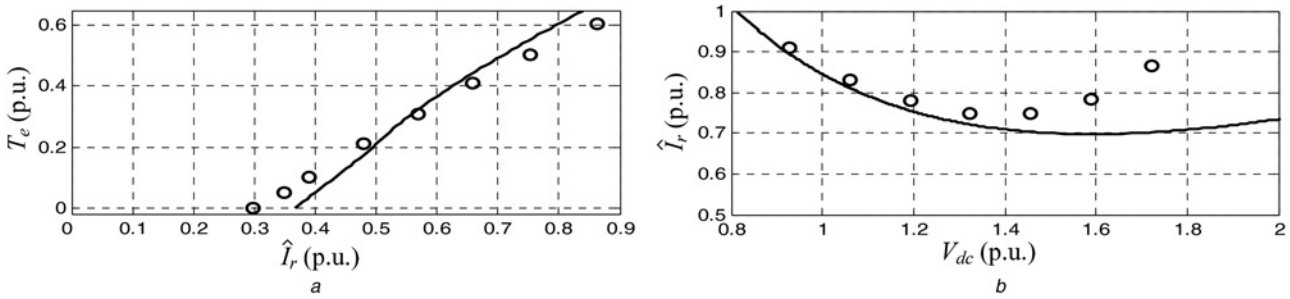

Fig. 9 *Theoretical steady-state characteristics (lines) at synchronism and experimental points (o)*
a $T_e(\hat{I}_R)$ characteristic with $V_{dc} = 9/2$
b $\hat{I}_R(V_{dc})$ characteristic with $T_e = 0.5$ pu (the rated optimal value of V_{dc} is $V_{dc} \simeq 1.432$ pu)

machine (prime mover), which is fed by a constant armature voltage.

Fig. 9*a* reports the steady-state torque against rotor current characteristic $T_e(\hat{I}_R)$ at synchronism and for a fixed $V_{dc} \simeq 1.432$ pu, according to (11), whereas Fig. 9*b* shows the characteristic $\hat{I}_R(V_{dc})$ at synchronism and for a fixed torque $T_e = 0.5$ pu. In both the figures, some experimental points (o) are shown together with the theoretical curves (continuous). The experimental value of $\hat{I}_R$ above which the diode bridge starts conducting is $\hat{I}_R \simeq 0.3$ pu, whereas the theory predicts 0.37 pu. This discrepancy is due to the fact that, in the incipient conduction condition, the peak line-to-line stator voltage equals the dc voltage: that is, $\sqrt{3}\omega_s L_s \hat{I}_R \simeq V_{dc}$. Thus, the no load stator voltage is $V_s = \omega_s L_s \hat{I}_R = V_{dc}/\sqrt{3} \simeq 1.432/\sqrt{3} = 0.83$ pu. Being the stator voltage lower than the rated value, the stator inductance is higher than the rated (slightly saturated) value (2.25 pu), so that a lower rotor current $\hat{I}_R$ is needed to establish the aforementioned incipient conduction ac voltage. Further causes of mismatch between the theoretical characteristic in Fig. 9*a* and the experimental points should be imputed to the stator resistance, which is not totally negligible in the considered machine and to the operation not strictly in CCM. As far as the characteristic $\hat{I}_R(V_{dc})$ in Fig. 9*b* is concerned, here the test is performed by keeping fixed the moving torque and by varying V_{dc} in a whole range. Thus, a noticeable change of L_s because of the saturation is expected at high V_{dc}: the higher is V_{dc}, the lower is L_s and the higher is the rotor (exciting) current needed to have the same stator voltage, with respect to the theoretical (almost unsaturated) value. The accuracy of the model could be improved by taking into account a variable stator inductance, which depends on the saturation. However, for the design purposes considered in this paper, the main interest is focused on the rated operation point, where an estimation of the rated value of the stator inductance can be used. The discrepancies are also because of the fact that the experimental system does not strictly operate in CCM, because the current control is not totally able to impose a sinusoidal rotor current, due in particular to the high sixth harmonic in the rotor back EMF produced by the diode switching. Nevertheless, the CCM assumption allows to find approximate results useful for the design of the DFIG.

7 Conclusion

The operation of a DFIG connected on the stator to a dc net by a diode rectifier and current controlled on the rotor has been studied by considering a simple control technique. This is an interesting layout for the connection of a WECS to a dc bus common to other sources or storages. To control the system, a rotating rotor current space vector at constant speed is imposed by the inverter: its amplitude is adjusted in order to regulate the average electromagnetic torque and thus also the power delivered to the dc bus. The impressed speed of the reference rotor current space vector determines the stator frequency. An analytical model for the steady-state analysis has been proposed and the most proper design specifications for the DFIG in this special application have been deduced. The theory has been validated by simulations. Experimental results showing the response to steps in the moving torque and in the reference speed have been reported to demonstrate that the control system is able to regulate the stator frequency and the rotor speed. Theoretical and experimental steady-state characteristics rotor current against torque and dc voltage have also been included.

8 Acknowledgments

This work was supported by the national funds through FCT – Fundação para a Ciência e a Technologia, under project PEst-OE/EEI/LA0021/2013.

9 References

1 Tazil, M., Kumar, V., Bansal, R.C., *et al.*: 'Three-phase doubly fed induction generators: an overview', *IET Electr. Power Appl.*, 2010, **4**, (2), pp. 75–89
2 Pena, R., Clare, J.C., Asher, G.M.: 'Doubly fed induction generator using back-to-back PWM converters and its application to variable-speed wind-energy generation', *Proc. Inst. Electr. Eng., Electr. Power Appl.*, 1996, **143**, pp. 231–241
3 Pena, R., Clare, J.C., Asher, G.M.: 'A doubly fed induction generator using back-to-back PWM converters supplying an isolated load from a variable speed wind turbine', *Proc. Inst. Electr. Eng., Electr. Power Appl.*, 1996, **143**, (5), pp. 380–387
4 Santos-Martin, D., Rodriguez-Amenedo, J.L., Arnalte, S.: 'Providing ride-through capability to a doubly fed induction generator under unbalanced voltage dips', *IEEE Trans. Power Electron.*, 2009, **24**, (7), pp. 1747–1757
5 Hu, S., Lin, X., Kang, Y., Zou, X.: 'An improved low-voltage ride through control strategy of doubly fed induction generator during grid faults', *IEEE Trans. Power Electron.*, 2011, **26**, (12), pp. 3653–3665
6 Rolan, A., Corcoles, F., Pedra, J.: 'Behaviour of the doubly fed induction generator exposed to unsymmetrical faults', *IET Electr. Power Appl*, 2012, **6**, (8), pp. 561–574
7 Wei, F., Zhang, X., Vilathgamuwa, M.D., Choi, S.S., Wang, S.: 'Mitigation of distorted and unbalanced stator voltage of stand-alone doubly fed induction generators using repetitive control technique', *IET Electr. Power Appl.*, 2013, **7**, (8), pp. 654–663
8 Xu, H., Hu, J., He, Y.: 'Operation of wind-turbine-driven DFIG systems under distorted grid voltage conditions: analysis and experimental validations', *IEEE Trans. Power Electron.*, 2012, **27**, (5), pp. 2354–2366

9 Hu, J., Nian, H., Xu, H., He, Y.: 'Dynamic modeling and improved control of DFIG under distorted grid voltage conditions', *IEEE Trans. Energy Convers.*, 2011, **26**, (1), pp. 163–175

10 Phan, V.T., Lee, H.H.: 'Stationary frame control scheme for a stand alone doubly fed induction generator system with effective harmonic voltages rejection', *IET Electr. Power Appl.*, 2011, **5**, (9), pp. 697–707

11 Cárdenas, R., Pena, R., Clare, J., Asher, G., Proboste, J.: 'MRAS observers for sensorless control of doubly-fed induction generators', *IEEE Trans. Power Electron.*, 2008, **23**, (3), pp. 1075–1084

12 Shen, S., Mwinyiwiwa, B., Zhang, Y., Ooi, B.T.: 'Sensorless maximum power point tracking of wind by DFIG using rotor position phase lock loop (PLL)', *IEEE Trans. Power Electron.*, 2009, **24**, (4), pp. 942–951

13 Kumar Jain, A., Ranganathan, V.T.: 'Wound rotor induction generator with sensorless control and integrate active filter for feeding nonlinear loads in a stand-alone grid', *IEEE Trans. Ind. Electron.*, 2008, **55**, (1), pp. 218–228

14 Carmeli, M.S., Castelli-Dezza, F., Iacchetti, M.F., Perini, R.: 'A MRAS observer applied to sensorless doubly fed induction machine drives'. IEEE Int. Symp. Industrial Electronics 2010 (ISIE '10), Bari – Italy, 5–7 July 2010

15 Forchetti, D., Garcia, G., Valla, M.I.: 'Adaptive observer for sensorless control of stand-alone doubly fed induction generator', *IEEE Trans. Ind. Electron.*, 2009, **56**, (10), pp. 4174–4180

16 Marques, G.D., Sousa, D.M.: 'Air-gap power vector based sensorless method for DFIG control without flux estimator', *IEEE Trans. Ind. Electron.*, 2011, **58**, (10), pp. 4717–4726

17 Blaabjerg, F., Chen, Z., Kjaer, S.B.: 'Power electronics as efficient interface in dispersed power generation system', *IEEE Trans. Power Electron.*, 2004, **19**, (5), pp. 1184–1194

18 Karlsson, P., Svensson, J.: 'DC bus voltage control for a distributed power system', *IEEE Trans. Power Electron.*, 2003, **18**, (6), pp. 1405–1412

19 Xu, L., Chen, D.: 'Control and operation of a DC microgrid with variable generation and energy storage', *IEEE Trans. Power. Deliv.*, 2011, **26**, (4), pp. 2513–2522

20 Kakigano, H., Miura, Y., Ise, T.: 'Low-voltage bipolar-type DC microgrid for super high quality distribution', *IEEE Trans. Power Electron.*, 2010, **25**, (12), pp. 3066–3075

21 Enamul Haque, Md., Negnevitsky, M., Muttaqi, K.M.: 'A novel control strategy for a variable-speed wind turbine with a permanent-magnet synchronous generator', *IEEE Trans. Ind. Appl.*, 2010, **46**, (1), pp. 331–339

22 Di Gerlando, A., Foglia, G., Iacchetti, M.F., Perini, R.: 'Simulations and test results of grid connected WECSs with diode rectifiers and modular PMSGs'. IEEE Int. Conf. Electrical Machines 2010 (ICEM '10), Roma – Italy, 6–8 September 2010

23 Vijayakumar, K., Kumaresan, N., Gounden, N.A.: 'Operation and closed-loop control of wind driven stand alone doubly fed induction generators using a single inverter-battery system', *IET Electr. Power Appl.*, 2012, **6**, (3), pp. 162–171

24 Marques, G.D., Iacchetti, M.F.: 'Inner control method and frequency regulation of a DFIG connected to a DC-link', accepted for publication on *IEEE Trans. Energy Convers.*, 2014, DOI:10.1109/TEC.2014.2299892

25 Holtsmark, N., Bahirat, H.J., Molinas, M., Mork, B.A., Hoidalen, H.K.: 'An all-DC offshore wind farm with series-connected turbines: an alternative to the classical parallel AC model?', *IEEE Trans. Ind. Electron.*, 2013, **60**, (6), pp. 2420–2428

26 Di Gerlando, A., Foglia, G.M., Iacchetti, M.F., Perini, R.: 'Comprehensive steady-state analytical model of a three-phase diode rectifier connected to a constant dc voltage source', *IET Power Electron.*, 2013, **6**, (9), pp. 1927–1938

27 Bleijs, J.A.M.: 'Continuous conduction mode operation of three-phase diode bridge rectifier with constant load voltage', *IEE Proc. Electr. Power Appl.*, 2005, **152**, (2), pp. 359–368

28 Mirecki, A., Roboam, X., Richardeau, F.: 'Comparative study of maximum power strategy in wind turbines'. Proc. IEEE Int. Symp. Industrial Electronics, 2004, pp. 993–998

29 Marques, G.D., Sousa, D.M.: 'Understanding the DFIG during voltage dips', *IEEE Trans. Energy Convers.*, 2012, **27**, (2), pp. 421–431

30 Pyrhonen, J., Jokinen, T., Hrabvocova, V.: 'Design of rotating electrical machines' (John Wiley & Sons, 2008) pp. 222

10 Appendix

DFIG used in the experimental tests: (stator Y/rotor Y) 380/185 V, 8/12.5 A, 3.75 kW, 50 Hz, 4 poles, turns ratio 2.05, $M = 2.13$ pu, $L_r = 2.25$ pu, $L_s = 2.27$ pu, $R_r = 0.071$ pu, $R_s = 0.057$ pu, inertia constant $H = 0.28$ s.

(Fictitious stator and rotor data in the exchanged connection: 185/380 V, 12.5/8 A, $n_{12} = 1/2.05 = 0.49$).